Remote Sens. **2011**, *3*, 1943-1956; doi:10.3390/rs3091943

OPEN ACCESS

Remote Sensing

ISSN 2072-4292

www.mdpi.com/journal/remotesensing

Article

A Multi-Resolution Multi-Temporal Technique for Detecting and Mapping Deforestation in the Brazilian Amazon Rainforest

Egídio Arai [1,*], Yosio E. Shimabukuro [1], Gabriel Pereira [1] and Nandamudi L. Vijaykumar [2]

[1] Remote Sensing Division, National Institute for Space Research, Av. dos Astronautas, 1758, Jardim da Granja, São José dos Campos, SP 12227-010, Brazil; E-Mails: yosio@dsr.inpe.br (Y.E.S.); gabriel@dsr.inpe.br (G.P.)

[2] Laboratory of Computing and Applied Mathematics, National Institute for Space Research, Av. dos Astronautas, 1758, Jardim da Granja, São José dos Campos, SP 12227-010, Brazil; E-Mail: vijay@lac.inpe.br

* Author to whom correspondence should be addressed; E-Mail: egidio@dsr.inpe.br; Tel.: +55-12-3208-6668; Fax: +55-12-3208-6488.

Received: 13 July 2011; in revised form: 11 August 2011 / Accepted: 19 August 2011 / Published: 1 September 2011

Abstract: The analysis of rapid environment changes requires orbital sensors with high frequency of data acquisition to minimize cloud interference in the study of dynamic processes such as Amazon tropical deforestation. Moreover, a medium to high spatial resolution data is required due to the nature and complexity of variables involved in the process. In this paper we describe a multiresolution multitemporal technique to simulate Landsat 7 Enhanced Thematic Mapper Plus (ETM+) image using Terra Moderate Resolution Imaging Spectroradiometer (MODIS). The proposed method preserves the spectral resolution and increases the spatial resolution for mapping Amazon Rainfores deforestation using low computational resources. To evaluate this technique, sample images were acquired in the Amazon rainforest border (MODIS tile H12-V10 and ETM+/Landsat 7 path 227 row 68) for 17 July 2002 and 05 October 2002. The MODIS-based simulated ETM+ and the corresponding original ETM+ images were compared through a linear regression method. Additionally, the bootstrap technique was used to calculate the confidence interval for the model to estimate and to perform a sensibility analysis. Moreover, a Linear Spectral Mixing Model, which is the technique used for deforestation mapping in Program for Deforestation Assessment in the Brazilian Legal Amazonia (PRODES) developed by National Institute for Space Research (INPE), was applied to analyze the differences in deforestation estimates. The results showed high

correlations, with values between 0.70 and 0.94 ($p < 0.05$, student's *t* test) for all ETM+ bands, indicating a good assessment between simulated and observed data ($p < 0.05$, Z-test). Moreover, simulated image showed a good agreement with a reference image, originating commission errors of 1% of total area estimated as deforestation in a sample area test. Furthermore, approximately 6% or 70 km² of deforestation areas were missing in simulated image classification. Therefore, the use of Landsat simulated image provides better deforestation estimation than MODIS alone.

Keywords: image simulation; deforestation; MODIS; Landsat 7

1. Introduction

Remote Sensing images have been used in studies and research in several areas, such as monitoring, mapping and management of vegetation resources [1–3], in the studies of the effects of floods [4,5], droughts [6,7], biomass burning [8–10], desertification [11,12], urban planning [13] and oceans characterization [14].

Recently, the number of environmental satellite sensors acquiring images of the earth's surface has been significantly increasing. However, the availability of these images is restricted due to limitations imposed by the satellites and characteristics of the sensors, such as spatial, spectral and temporal resolutions. Also, an important factor to be considered when using satellite images of optical remote sensing is the presence of clouds that reduces the number of images available for environmental analysis. An example of cloud-free derived data limitation can be observed in the Program for Deforestation Assessment in the Brazilian Legal Amazonia (PRODES) developed by the National Institute for Space Research (INPE). During the rainy season, the lack of images of medium and high spatial resolution is evident due to persistent cloud cover that reduces the fraction of usable data per image.

Since the results are annual, the mapping of deforestation carried out by PRODES is insufficient to provide an inventory for government mitigation. To solve this problem, the Government program for Deforestation Detection in Real Time (DETER) was created using MODIS images, allowing near real-time tracking of deforestation, to act as a warning system. However, limitations in using MODIS images are related to its spatial resolution (only polygons with more than 25 hectares are detected) which underestimate the total deforestation area.

In the literature, several techniques of image processing have been widely proposed to improve the spatial resolution of remote sensing images, such as image fusion and super-resolution techniques [15–22]. However, image fusion techniques, such as Brovey Transform, Intensity-Hue-Saturation (IHS) and Principal Component Analysis (PCA), spectrally deform the images, altering the radiometric values and histograms. Also, some methods restrict the number of images involved in the process [23] and restrict the size of images, such as wavelets transform [24]. Moreover, super-resolution techniques need a sequence of images over the same location without significant alterations [25], which is not recommended for deforestation estimates.

Frequently, a fusion of remote sensing image methods can be employed to merge high spatial panchromatic with low spatial multispectral images. These techniques are not appropriate for dynamic studies as they require high temporal resolution images [26] and, under persistent cloud cover, preclude the acquisition of data. Optical remote sensing images with medium/high spatial resolution used in deforestation estimates, such as the Brazilian PRODES project (www.obt.inpe.br/prodes), which utilizes images from Thematic Mapper (TM) and Enhanced Thematic Mapper Plus (ETM+) sensors onboard the Landsat satellites series [2], have limitations during the rainy season due to the non-availability of cloud-free images because of their low temporal resolution [27,28]. However, high temporal resolution imagery is required for an alarm system to inform federal agencies to take timely action against illegal clearing.

In this context, the alternative to low frequency observations such as those provided by Landsat is to use data from MODIS. The high temporal resolution increases the probability of acquiring cloud free images and facilitates the deforestation estimation during the rainy season. Furthermore, an alternative is to merge high spatial resolution imagery with high temporal resolution imagery to simulate frequent high spatial resolution imagery. Thus, the main objective of this work is to simulate ETM+ image using MODIS sensor data, improving both temporal and spatial resolutions and at the same time preserving the spectral resolution.

2. Materials

2.1. Study Site

The study site for this work is located in the State of Mato Grosso in Brazilian Amazon. This region is composed by a plateau and plains in the center, plain land with swamps at west and dips and plateaus in the north side. The climate of Mato Grosso could be described as Am, according to the Köppen classification, due to the tropical climate with annual temperature average exceeding 26 °C. The rainfall is also high, reaching 2,000 mm per year with a rainy summer and a dry winter. Mato Grosso State has experienced much deforestation in recent years, as can be observed from the data obtained by the PRODES (http://www.obt.inpe.br/prodes/) project from 1995 to 2008 (Figure 1).

2.2. Remote Sensing Images

For this work, one scene from the Landsat ETM+ sensor (227/68) acquired on 17 July 2002 and daily surface reflectance images from the MODIS sensor from the Terra platform acquired on 17 July 2002 and 05 October 2002 were used. The difference in image acquisition between Terra (temporal resolution of 2 days) and Landsat 7 (temporal resolution of 16 days) platforms is about 30 minutes (Landsat 7 and Terra crosses the equator at approximately 10:00 AM and 10:30 AM, respectively).

The ETM+/Landsat 7 has 8 bands, in which 6 bands are multispectral (referring to blue, green, red, near infrared and two short wave infrared), one thermal band and one panchromatic band with 30 m, 60 m and 15 m, respectively.

The MOD09 product of MODIS sensor used in this work is an estimate of the spectral surface reflectance for each one of the first 7 land spectral bands [29] as described in Table 1. This product is obtained through the measured signal by the instrument on the top of the atmosphere

(Top-of-Atmosphere-TOA), which performs corrections of molecular scattering, absorption of gases and effects of aerosols. The procedure of atmospheric correction uses the Second Simulation of the Satellite Signal in the Solar Spectrum (6S) radiative transfer model, which was simplified for operational applications for the MODIS surface reflectance product [30].

Figure 1. (a) Study area located in Mato Grosso State, Brazilian Amazon, corresponding to the Path 227/Row 68 of Enhanced Thematic Mapper Plus (ETM+) Landsat 7; and **(b)** annual deforestation estimates of Mato Grosso.

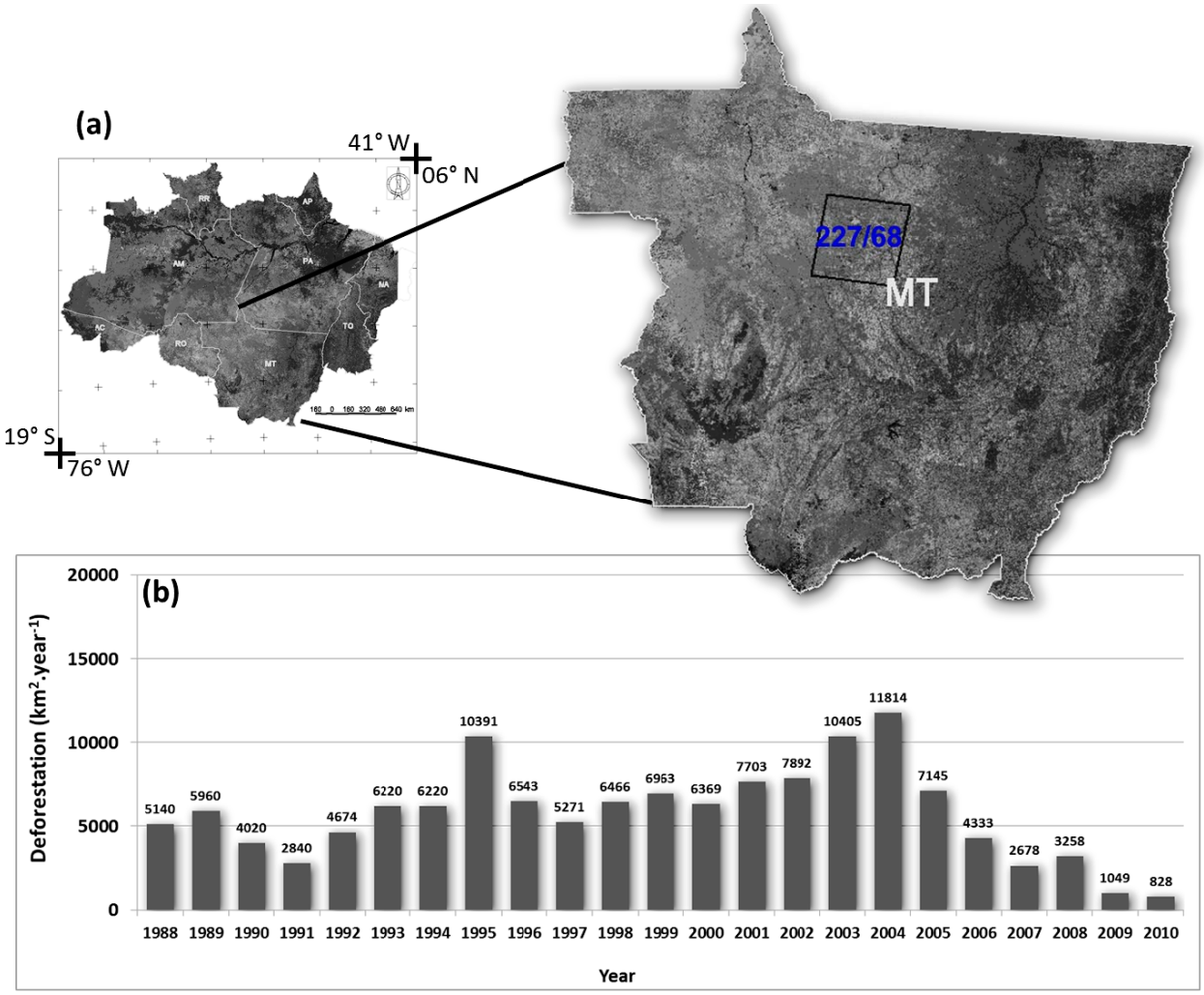

Table 1. Comparison of the ETM+ and Terra Moderate Resolution Imaging Spectroradiometer (MODIS) bands.

ETM+/L7 Band	ETM+/L7 bandwidth (nm)	MODIS/Terra Band	MODIS/Terra bandwidth (nm)	ETM+/L7 spatial resolution (m)	MODIS/Terra spatial resolution (m)
1	450–515	3	459–479	30	500
2	525–605	4	545–565	30	500
3	630–690	1	620–670	30	250
4	775–900	2	841–876	30	250
5	1,550–1,750	6	1,628–1,652	30	500
7	2,090–2,350	7	2,105–2,155	30	500

3. Methods

3.1. Pre-Processing

The ETM+ image was geometrically corrected using manually selected control points to fit and apply a first order polynomial and a nearest neighbor resampling. The resulting root mean square error was less than 0.5 pixels.

The ETM+ multispectral bands were converted to surface reflectance using the Second Simulation of the Satellite Signal in the Solar Spectrum (6S) transfer model [31]. In the 6S modulation of atmosphere interference, the visibility of 70 km, the tropical atmosphere and the continental aerosol models were adopted as initial conditions. It was assumed that the main effects of the atmosphere would be: absorption by water vapor, carbon dioxide, oxygen and ozone and the atmospheric scattering by gases and aerosol molecules.

3.2. Methodological Approach

The methodology described here shows the simulation of each ETM+ band image using MODIS image, preserving the spectral resolution of 30 m. The ETM+ sensor acquires images every 16 days at 10:00 A.M. whereas, due to the fact that MODIS acquires images every two days (close to daily) at 10:30 A.M., the difference in daily simultaneous image acquisition does not have a significant influence in merging image processing results because changes in the atmosphere and in land surface are not substantial. In order to make the ETM+ data compatible with MOD09 product, the values of surface reflectance are derived.

Multispectral ETM+ images have a spatial resolution of 30m, while MODIS has a spatial resolution of 250 m and 500 m, depending on the spectral band analyzed. Thus, a MODIS pixel covers around 69 and 278 pixels of ETM+, respectively. Assuming that the pixel composition of an image is a mixture of the spectral responses of the target that compose the imaged area, it is possible to conclude that the spectral signal captured in a MODIS pixel is the combination of the spectral signatures of the ETM+ pixels covering the MODIS pixel. In addition, assumptions in fusion methods might introduce several sources of errors such as geometrical differences due to registration process [32] and changes in scene illumination based on sun azimuth and elevation that alters the orientation and size of shadows [33,34]. Furthermore, we assumed that a rectangular Modulation Transfer Function (MTF) interpolating a MODIS pixel to a finer spatial scale of Landsat would make one MODIS pixel cover exactly n × n Landsat pixels.

Figure 2 shows the procedure, which takes advantage of the temporal resolution of MODIS and spatial resolution of ETM+. The methodology developed in this work could be divided into two steps (Equations (1) and (2)). The first step consists of estimating the mask of ETM+ percentage contribution (weight matrix) through a comparison between MODIS and ETM+ pixels for the same acquisition day. In this step, for each band of a Reference Date (RD), ETM+ image, represented as a matrix of m rows by n columns (ETMRD(m,n)), is compared with respective MODIS pixel value (MODIS_PVRD). Then, a mask of ETM+ percentage contribution is generated by the ratio of ETMRD(m,n) and MODIS_PVRD. The second step is related to the merger of MODIS pixel value Target Date (MODIS_PVTD) and the calculated ETM+ percentage contribution mask. In this step,

new MODIS image from other date are multiplied by the obtained mask to get a simulated 30 m spatial resolution image.

$$ETM+_{Contribution}(m,n) = ETM_{RD}(m,n)/MODIS_{PVRD}(x,y) \quad (1)$$

$$\text{Image Result}(m,n) = ETM+_{Contribution}(m,n) * MODIS_{PVTD}(x,y) \quad (2)$$

Figure 2. Methodological procedure to originate the mask of the contribution of ETM+ pixels to the corresponding MODIS reference date pixel (Step 1), and to originate the image by application of the mask in MODIS target date pixel.

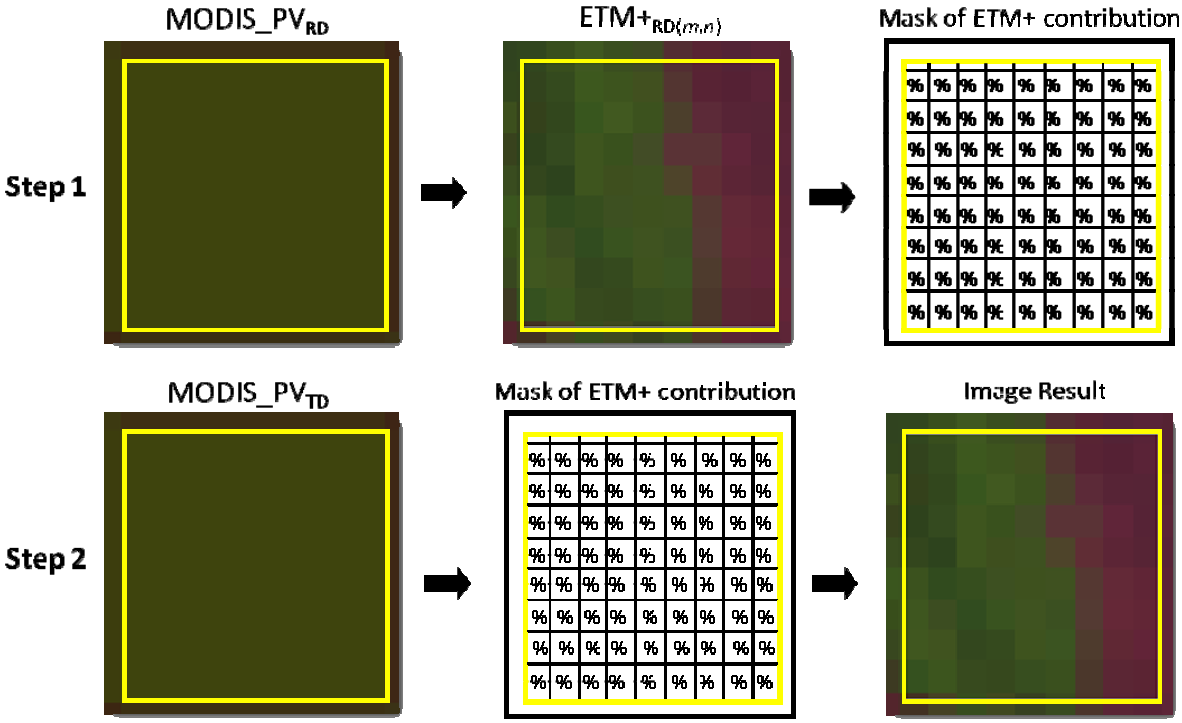

3.3. Linear Spectral Mixing Model (LSMM)

The LSMM is used by PRODES to map deforestation and was applied in this work for comparison in detecting deforestation. The variability of spectral response that forms each pixel depends on the spatial resolution of each sensor. Consequently, pixels of high spatial resolution sensors have a higher probability of being formed by single targets with similar physical-chemical and biological properties, or pure pixels. This feature does not occur in pixels of coarse resolution sensors, in which spectral mixture is variable and could mask the spectral response characteristics of each target, not enabling their identification.

In this work, pure pixels, also called endmembers, used as input in LSMM were selected directly from MODIS and ETM+/Landsat 7 images. In this procedure, pixels with spectral response closer to the theoretical curve expected were selected as pure targets. The endmembers for each image are composed of vegetation, soil and shade fraction. Thus, the value of a certain pixel in a scene can be described as:

$$\rho_i = a.veg_i + b.soil_i + c.shade_i + e_i \quad (3)$$

where ρ_i represents the pixel surface reflectance at band *i*; *a*, *b* and *c* corresponding to vegetation, soil and shade fraction in a pixel, respectively; veg_i, $soil_i$ and $shade_i$ are the spectral response of vegetation, soil and shade components, respectively; and e_i represents the error in band *i*.

3.4. Image Classification and Statistical Analysis

In this work, we used the ISOSEG classifier algorithm available in SPRING [35], a geographic information system developed by the Brazilian Institute for Space Research, to separate the regions of a segmented image with a similarity of eight and a minimal area of 12 pixels. The ISOSEG classifier is a clustering algorithm for unsupervised data, applied to a set of regions, which in turn are characterized by their statistical attributes such as mean and covariance matrix, and also by area.

The ISOSEG algorithm for clustering assumes no prior knowledge of the probability density distribution of the subjects. It is a technique that seeks to classify the cluster regions, as a measure of similarity between them. The similarity measure used is the Mahalanobis distance between the class and the candidate regions of relevance with respect to this class. To obtain the thematic maps, the soil fractions generated by Linear Spectral Mixing Model (LSMM) were classified in forest/non-forest by the ISOSEG classifier.

The validation of this methodology compared the simulated and the corresponding original ETM+ image using a linear regression method. Also, the Bootstrap technique developed by [36] was used to calculate the confidence interval for the model estimate and a Linear Spectral Mixing Model [2,37] was applied to analyze the differences in deforestation estimate. The accuracy of thematic maps resulting from ISOSEG classifications were statistically tested using the Kappa index [38].

The Kappa statistic is a method of assessing the correlation between two or more classifications. The advantage of the Kappa statistics is that, in calculating the coefficient, it includes all elements of the error matrix and not only the main diagonal elements, as in the global accuracy. Equation 4 is used to determine the Kappa value [39,40]:

$$\hat{K} = \frac{N\sum_{i=1}^{r} x_{ij} - \sum_{i=1}^{r}(x_i + x_{+i})}{N^2 - \sum_{i=1}^{r}(x_i + x_{+i})} \quad (4)$$

where *K* is the estimator of Kappa coefficient; *r* is the number of rows of square matrix; x_{ij} is the number of observations in row *i* and column *j*, respectively; and *N* is the number of observations.

4. Results and Discussion

Figure 3(a,b) shows ETM+ and MODIS reference images acquired on 17 July 2002, corresponding to the 227/68 Landsat 7 scene, respectively. The mask of ETM+ contribution, derived from these images, was applied on the MODIS image of 05 October 2002 (Figure 3(c)) as described in step 2 to simulate the ETM+ image of the same date (Figure 3(d)).

Moreover, while other fusion methods that merge remote sensing images modify the spectral resolution, such as IHS, the method proposed in this work shows a good conformance in preserving the surface reflectance of ETM+ pixels. Also, the improvement of spatial resolution can be observed on the roads and drainage net, as well as the borders of the deforested areas. It is remarkable that this

multiresolution multitemporal blending technique requires only one ETM+/Landsat 7 and MODIS reference date image. From these reference images, the derived mask of ETM+ percentage contribution can be applied successively in MODIS target images to simulate the corresponding ETM+ images of distinct dates.

Figure 3. (a) ETM+ reference date of 17 July, 2002 (3B4G5R); **(b)** MODIS reference date of 17 July 2002 (1B2G6R); **(c)** MODIS 05 October, 2002 target date image (1B2G6R); **(d)** ETM+ image of 05 October, 2002 (3B4G5R); and **(e)** MODIS-based simulated ETM+ image of 05 October 2002 (3B4G5R).

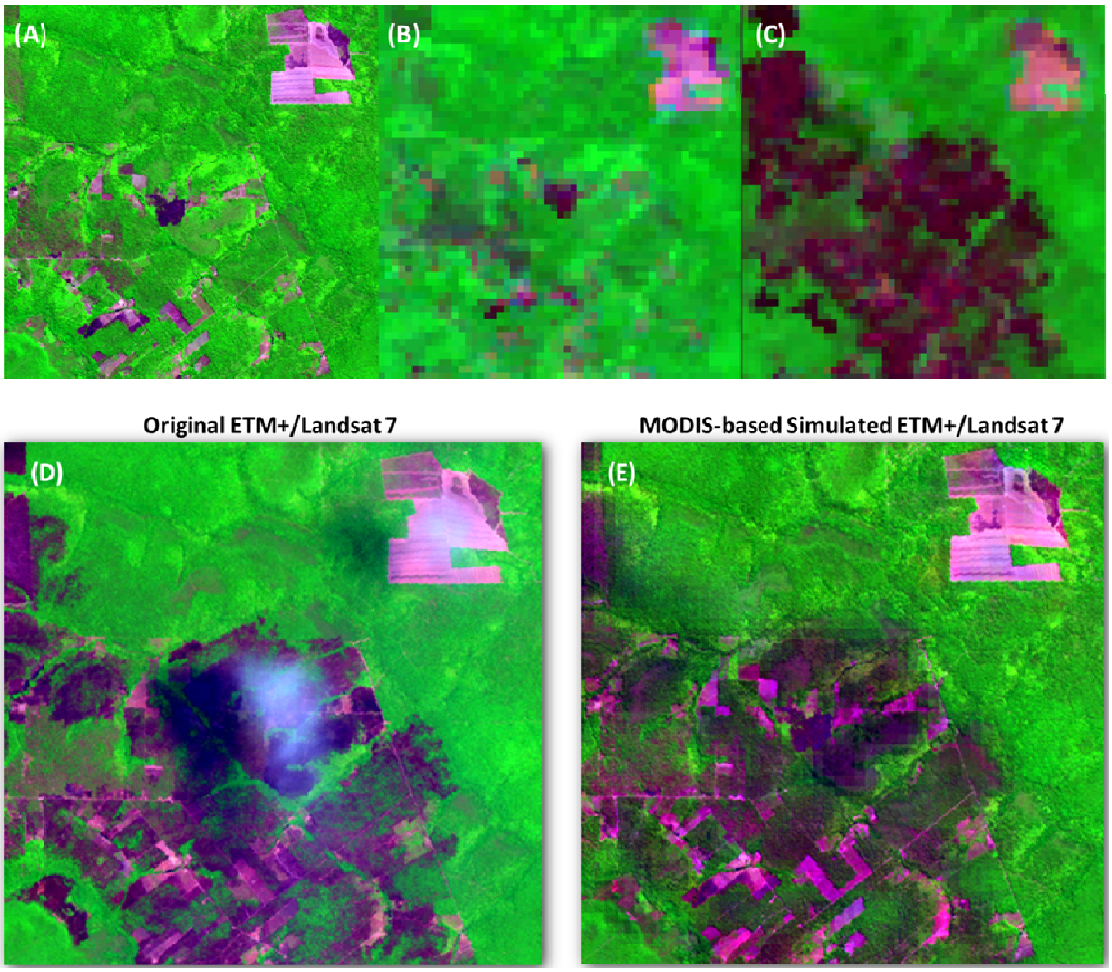

Figure 4 shows the linear regression and respective correlation distributions, between the surface reflectance ETM+/Landsat 7 acquired on 05 October, 2002 images (x-axis) and MODIS-based simulated ETM+ images for the same date (y-axis), using the bootstrap technique developed by [36]. In this method, a population of 1.0×10^4 reconstructs the original curve and provides the parameters to create the confidence interval for the model estimate.

As shown in Figure 4(a–c), the highest frequencies of correlations for bands 1, 2, and 3 are between 0.65–0.75, 0.80–0.85 and 0.90–0.93 ($p < 0.05$, student's *t*-test), respectively. Furthermore, the confidence interval for the slope and offset samples histogram distribution of these bands are between 0.90–1.25 and −9 to −10, respectively. Figure 4(d–f) shows correlations frequencies of 0.70–0.80, 0.92–0.94 and 0.92–0.95 ($p < 0.05$, student's *t*-test) for bands 4, 5 and 7, respectively. Also, the near-

infrared band presented a slope between 0.55 and 0.65 with an offset centered in 2.5. The confidence interval for the slope samples histogram distribution of shortwave infrared (SWIR) bands is between 1.05 and 1.15 with an offset among −3 and −1.

The low correlation frequencies found between ETM+ and MODIS-based simulated ETM+ images in band 1 and band 4 probably occurred because of the major influence of scattering effects of the atmosphere in the blue region of the electromagnetic spectrum and due to the effect of texture caused by trees canopy in NIR band, respectively.

Figure 4. Linear Regression and slope distributions using the bootstrap technique developed by [36] for shortwave ETM+/Landsat 7 and MODIS-based simulated ETM+ bands.

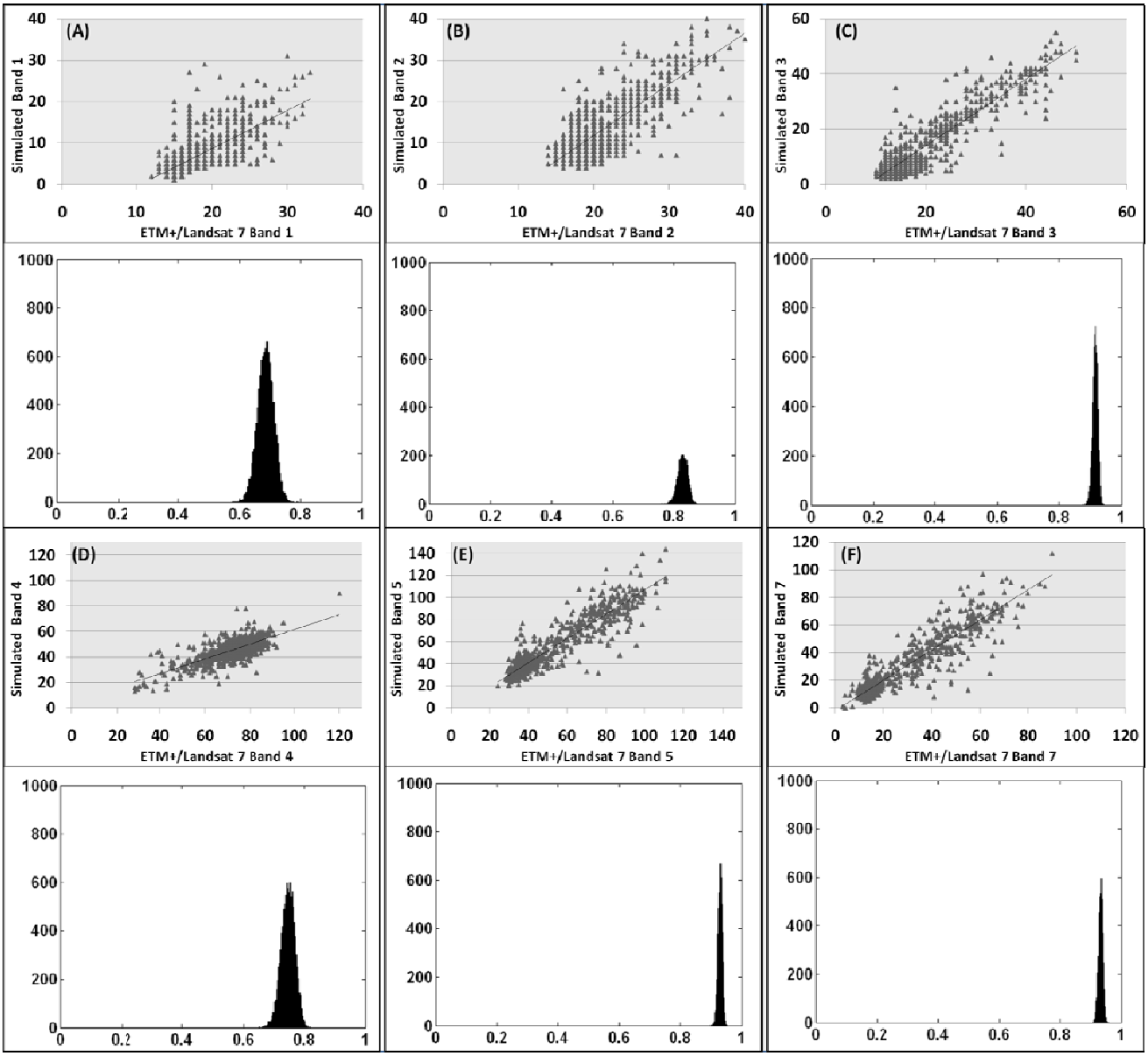

In order to compare the results, an ETM+ image from 05 October 2002 was used and Figure 5 shows subset images classifications to 05 October 2002 ETM+ image (Figure 5(a)), 05 October 2002 MODIS-based simulated ETM+ image (Figure 5(b)) and 05 October 2002 MODIS image (Figure 5(c)).

The classification results show that MODIS-based simulated ETM+ classification (Figure 5(b)) reveal a good agreement with the results obtained by original ETM+ classification (Figure 5(a)). Comparing total area classified as deforestation and vegetated areas (Table 2), the original ETM+/Landsat 7 image from 05 October 2002 estimated approximately 4,700 km^2 of deforestation areas and 1,440 km^2 of areas with vegetation (including Amazon rainforest, grassland and other types of land use). The MODIS image for the same day of ETM+/Landsat 7 (05 October 2002) estimated 4,410 km^2 and 1,730 km^2 of deforestation and vegetated areas, respectively.

Figure 5. 05 October 2002, Isoseg classifications of soil fraction images: **(a)** ETM+ image; **(b)** MODIS-based simulated ETM image; **(c)** MODIS image.

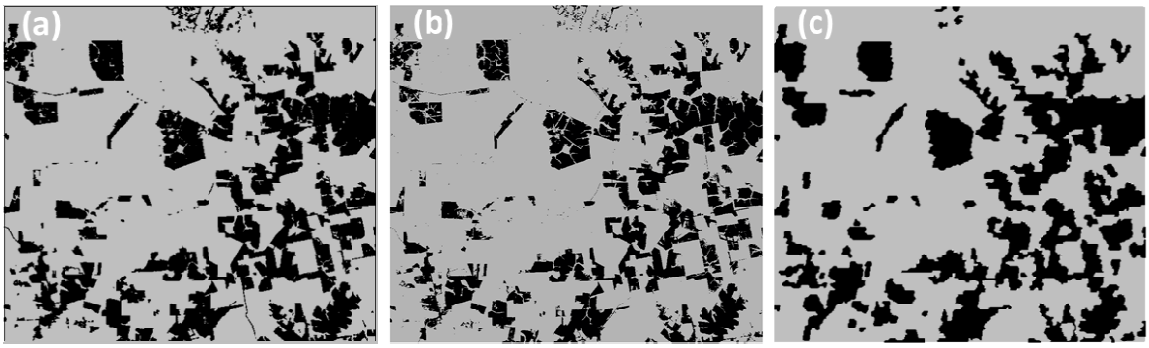

Table 2. Deforestation and vegetated areas estimation and omission commission errors for 05 October 2002.

Sensor/Classification	ETM+/L7 (km^2)	MODIS/Terra (km^2)	Simulated Image (km^2)
Deforestation	4,700.8	4,410.3	4,768.6
Vegetated areas	1,440.3	1,730.8	1,372.5
Omission	-	10%	6%
Commission	-	9%	1%

Using the methodology developed in this work, the 05 October 2002 simulated image, originated from the weight matrix derived from ETM+/Landsat 7 and MODIS surface reflectance images acquired on 17 July 2002 estimates the deforestation of 4,768 km^2 and vegetated areas of 1,372 km^2. These values show a good agreement with original ETM+/Landsat 7 image.

To statistically compare the results of the classifications, a test was performed using a Z statistic calculated on the basis of kappa values and their respective variances [38]. In the first evaluation (ETM+ classification and simulated image classification), the obtained kappa value was 0.91 with an error of approximately 6% in deforestation underestimate. In the second analysis (ETM+ classification and MODIS classification), the kappa value was 0.75 with an error of approximately 20% in deforestation overestimate. Furthermore, the calculated value for Z-test ($p < 0.05$) indicates that statistically significant differences are evidenced between the kappa indices and, consequently, between the classifications.

Relating to omission and commission errors, the MODIS image showed a tendency to overestimate the deforestation, basically classifying areas of forest logged and burned as deforested area. In this

analysis, approximately 13% of the total deforested areas estimated by MODIS image were classified as Amazon rainforest in the reference image. Also, 11% of deforestation areas were missing in the MODIS estimation. Moreover, the simulated image showed an exceptional assessment with respect to the reference image. Commission errors represented only 1% of total area estimated as deforestation, occurring mainly in the borders of plots. Furthermore, approximately 6% or 70 km^2 of deforestation areas were missing in the simulated image classification. These errors occurred mainly in the dark objects of an image, such as recent biomass burnt scars and degraded forests areas.

5. Conclusions

The results obtained by the proposed method present a potential for INPE's deforestation detection activities such as DETER and PRODES by enhancing not only the contrast between forest and deforested areas, but also allowing a better area estimation.

The advantages of this low computational requirement method when compared to other fusion techniques are: the improvement of the spatial resolution, the unlimited number of bands and the size involved in multiresolution multitemporal blending techniques. Also, linear regressions and correlation histogram distributions show a good conformance in preserving the surface reflectance and in forest and non-forest estimates through LSMM.

This multiresolution multitemporal fusion technique shows promising results for accuracy development and upgrades could be developed to minimize the source of errors related to the MODIS point spread function and MODIS viewing angle.

Acknowledgments

The authors acknowledge the financial support from CAPES and FAPESP (2010/07083-0).

References

1. Myneni, R.B.; Keeling, C.D.; Tucker, C.J.; Asrar, G.; Nemani, R.R. Increased plant growth in the northern high latitudes from 1981 to 1991. *Nature* **1997**, *386*, 698–702.
2. Shimabukuro, Y.E.; Batista, G.T.; Mello, E.M.K.; Moreira, J.C.; Duarte, V. Using shade fraction image segmentation to evaluate deforestation in Landsat Thematic Mapper images of the Amazon Region. *Int. J. Remote Sens.* **1998**, *19*, 535–541.
3. Rogan, J.; Franklin, J.; Roberts, D.A. A comparison of methods for monitoring multitemporal vegetation change using Thematic Mapper imagery. *Remote Sens. Environ.* **2002**, *80*, 143–156.
4. Hess, L.L.; Melack, J.M.; Filsos, S.; Wang, Y. Delineation of inundated area and vegetation along the Amazon floodplain with the SIR-C synthetic aperture radar. *IEEE Trans. Geosci. Remote Sens.* **1995**, *334*, 896–904.
5. Sakamoto, T.; Nguyen, N.V.; Kotera, A.; Ohno, H.; Ishitsuka, N.; Yokozawa, M. Detecting temporal changes in the extent of annual flooding within the Cambodia and the Vietnamese Mekong Delta from MODIS time-series imagery. *Remote Sens. Environ.* **2007**, *109*, 295–313.
6. Mcvicar, T.R.; Bierwirth, P.N. Rapidly assessing the 1997 drought in Papua New Guinea using composite AVHRR imagery. *Int. J. Remote Sens.* **2001**, *22*, 2109–2198.

7. Singh, R.P.; Roy, S.; Kogan, F. Vegetation and temperature condition indices from NOAA AVHRR data for drought monitoring over India. *Int. J. Remote Sens.* **2003**, *24*, 4393–4402.
8. Roy, D.P.; Giglio, L.; Kendall, J.D.; Justice, C.O. A multitemporal active-fire based burn scar detection algorithm. *Int. J. Remote Sens.* **1999**, *20*, 1031–1038.
9. Giglio, L.; Descloitres, J.; Justice, C.O.; Kaufman, Y. An enhanced contextual fire detection algorithm for MODIS. *Remote Sens. Environ.* **2003**, *87*, 273–282.
10. Pereira, G.; Freitas, S.R.; Moraes, E.C.; Ferreira, N.J. Shimabukuro, Y.E.; Rao, V.B.; Longo, K.M. Estimating trace gas and aerosol emissions over South America: Relationship between fire radiative energy released and aerosol optical depth observations. *Atmos. Environ.* **2009**, *43*, 6388–6397.
11. Tucker, C.J.; Choudhury, B.J. Satellite remote sensing of drought conditions. *Remote Sens. Environ.* **1987**, 243–251.
12. Nemani, R.R.; Keeling, C.D.; Hashimoto, H.; Jolly, W.M.; Piper, S.C.; Tucker, C.J.; Myneni, R.B.; Running, S.W. Climate-driven increases in global terrestrial net primary production from 1982 to 1999. *Science* **2003**, *300*, 1560–1563.
13. Thomas, N.; Hendris, C.; Congalton, R.G. A comparison of urban mapping methods using high-resolution digital imagery. *Photogramm. Eng. Remote Sens.* **2003**, *69*, 963–972.
14. Emery, W.J.; Yu, Y. Satellite sea surface temperature patterns. *Int. J. Remote Sens.* **1997**, *18*, 323–334.
15. Hirosawa, Y.; Marsh, S.E.; Kliman, D.H. Application of standardized principal component analysis to land-cover characterization using multitemporal AVHRR data. *Remote Sens. Environ.* **1996**, *58*, 267–281.
16. Bajjouk, T.; Populus, J.; Guillaumont, B. Quantification of subpixel cover fractions using principal component analysis and a linear programming method: Application to the coastal zone of Roscoff (France). *Remote Sens. Environ.* **1998**, *64*, 153–165.
17. Tatem, A.J.; Lewis, H.G.; Atkinson, P.M.; Nixon, M.S. Super-resolution land cover pattern prediction using a Hopfield neural network. *Remote Sens. Environ.* **2002**, *79*, 1–14.
18. Kasetkasem, T.; Arora, M.K.; Varshney, P.K. Super-resolution land cover mapping using a Markov random field based approach. *Remote Sens. Environ.* **2005**, *96*, 302–314.
19. Zhang, Y.; Hong, G. An IHS and wavelet integrated approach to improve pan-sharpening visual quality of natural colour IKONOS and QuickBird images. *Inf. Fusion* **2005**, *6*, 225–234.
20. Gao, F.; Masek, J.; Schwaller, M.; Hall, F. On the blending of the Landsat and MODIS surface reflectance: Predicting daily Landsat surface reflectance. *IEEE Trans. Geosci. Remote Sens.* **2006**, *8*, 2207–2218.
21. Ling, Y.; Ehlers, M.; Usery, E.L.; Madden, M. FFT-enhanced IHS transform method for fusing high-resolution satellite images. *ISPRS J. Photogramm.* **2007**, *61*, 381–392.
22. Pal, S.K.; Majumdar, T.J.; Bhattacharya, A.K. ERS-2 SAR and IRS-1C LISS III data fusion: A PCA approach to improve remote sensing based geological interpretation. *ISPRS J. Photogramm.* **2007**, *61*, 281–297.
23. Pohl, C.; Genderen, J.L. Multisensor image fusion in remote sensing: Concepts, methods and applications. *Int. J. Remote Sens.* **1998**, *19*, 823–854.

24. Garguet-Duport, B.; Girel, J.; Chassery, J.M.; Pautou, G. The use of multiresolution analysis and wavelets transform for merging SPOT panchromatic and multispectral image data. *Photogramm. Eng. Remote Sensing* **1996**, *62*, 1057–1066.
25. Elad, M.; Feuer, A. Restoration of a single superresolution image from several blurred, noisy, and undersampled measured images. *IEEE Trans. Image Process.* **1997**, *6*, 1646–1658.
26. Laporterie, F.; Amram, O.; Flouzat, G.; Pilicht, E.; Gayt, M. Data Fusion Thanks to an Improved Morphological Pyramid Approach: Comparison Loop on Simulated Images and Application to SPOT 4 Data. In *Proceedings of the IEEE 2000 International Geoscience and Remote Sensing Symposium, IGARSS 2000*, Honolulu, HI , USA, 24–28 July 2000;Volume 5, pp. 2117–2119.
27. Asner, G.P. Cloud cover in Landsat observations of the Brazilian Amazon. *Int. J. Remote Sens.* **2001**, 22, 3855–3862.
28. Ju, J.; Roy, D.P. The availability of cloud-free Landsat ETM+ data over the conterminous United States and globally. *Remote Sens. Environ.* **2008**, *112*, 1196–1211.
29. Justice, C.O.; Vermote, E.F.; Townshend, J.R.G.; Defries, R.; Roy, D.P.; Hall, D.K.; Salomonson, V.V.; Privette, J.L.; Riggs, G.; Strahler, A.; *et al*. The moderate resolution imaging spectroradiometer (MODIS): Land remote sensing for global change research. *IEEE Trans. Geosci. Remote Sens.* **1998**, *36*, 1228–1249.
30. Vermote, E.F.; El Saleous, N.Z.; Justice, C.O. Atmospheric correction of MODIS data in the visible to middle infrared: First results. *Remote Sens. Environ.* **2002**, *83*, 97–111.
31. Vermote, E.F.; Tanre, D.; Deuze, J.L.; Herman, M.; Morcrette J.J. Second simulation of the satellite signal in the solar spectrum, 6S: An overview. *IEEE Trans. Geosci. Remote Sens.* **1997**, *35*, 675–686.
32. Blanc, P.; Wald, L.; Ranchin, T. Importance and Effect of Coregistration Quality in an Example of 'Pixel to Pixel' Fusion Process. In *Proceedings of the 2nd Conference Fusion Earth Data: Merging Point Measurements, Raster Maps and Remotely Sensed Images*, Sophia, Antipolis, France, 28–30 January 1998; pp. 67–73.
33. Thomas, C.; Ranchin, T.; Wald, L.; Chanussot, J. Synthesis of multispectral images to high spatial resolution: A critical review of fusion methods based on remote sensing physics. *IEEE Trans. Geosci. Remote Sens.* **2008**, *46*, 1301–1312.
34. Wolfe, R.E.; Roy, D.P.; Vermote, E. MODIS land data storage, gridding and compositing methodology: Level 2 grid. *IEEE Trans. Geosci. Remote Sens.* **1998**, *36*, 1324–1338.
35. Camara, G.; Souza, R.C.M.; Freitas, U.M.; Garrido, J. SPRING: Integrating remote sensing and GIS by object-oriented data modeling. *Comput. Graph.* **1996**, *20*, 395–403.
36. Efron, B. *The Jackknife, the Bootstrap, and Other Resampling Plans*; Society of Industrial and Applied Mathematics CBMS-NSF: Philadelphia, PA, USA, 1982.
37. Shimabukuro, Y.E.; Smith, J.A. The least-squares mixing models to generate fraction images derived from remote sensing multispectral data. *IEEE Trans. Geosci. Remote Sens.* **1991**, *29*, 16–20.
38. Congalton, R.G.; Mead, R.A. A review of three discrete multivariate analysis techniques used in assessing the accuracy of remotely sensed data from error matrices. *IEEE Trans. Geosci. Remote Sens.* **1986**, *24*, 169–174.

39. Congalton, R.G.; Green, K. *Assessing the Accuracy of Remotely Sensed Data: Principles and Practics*; CRC Press: New York, NY, USA, 1998.
40. Smits, P.C.; Dellepiane, S.G.; Schowengerdt, R.A. Quality assessment of image classification algorithms for land-cover mapping: A review and a proposal for a cost based approach. *Int. J. Remote Sens.* **1999**, *20*, 1461–1486.